One-dimensional method of investigating the localized states in armchair graphene-like nanoribbons with defects*

Yang Xie(谢阳), Zhi-Jian Hu(胡智健), Wen-Hao Ding(丁文浩), Xiao-Long Lü(吕小龙), and Hang Xie(谢航)†

College of Physics, Chongqing University, Chongqing 401331, *China*

(Received 20 July 2017; revised manuscript received 12 September 2017; published online 20 November 2017)

In this paper we propose a type of new analytical method to investigate the localized states in the armchair graphene-like nanoribbons. The method is based on the tight-binding model and with a standing wave assumption. The system of armchair graphene-like nanoribbons includes the armchair supercells with arbitrary elongation-type line defects and the semi-infinite nanoribbons. With this method, we analyze many interesting localized states near the line defects in the graphene and boron-nitride nanoribbons. We also derive the analytical expressions and the criteria for the localized states in the semi-infinite nanoribbons.

Keywords: graphene nanoribbons, tight-binding model, energy band, localized states

PACS: 73.22.Pr, 72.80.Vp, 71.15.–m **DOI:** 10.1088/1674-1056/26/12/127310

1. Introduction

Graphene, as a novel two-dimensional material, has attracted a lot of research interest in this decade since it was discovered in 2003.[1] It has many special electronic, optic and magnetic properties due to its energy band structure.[2,3] For example, graphene has the Dirac-like electron with the Klein tunneling effect.[4,5] It has the half integer quantum Hall effect.[6]

With the restriction of one dimension, the bulk graphene forms the graphene nanoribbons (GNR). Armchair GNR (aGNR) and zigzag GNR (zGNR) are the two basic types.[7] There are edge states on the edges of the zGNR.[7] The early tight binding (TB) model shows that these edge states appear near the Fermi level with a large density of states.[7,8] With the Hubbard model and the first-principles calculations, it is found that these edge states actually have an energy gap near the Fermi level with opposite spin polarizations on two edges.[9,10] Some half-metal structures can be prepared by the atom modulations in zGNR systems.[11–13] Furthermore, the properties of some complex structures, such as the transport properties of the double-layer graphene with line defects, the graphene superlattice and doubly-stacked zGNR have been studied by many methods.[14–16] In the thermal physics aspect, there are also a lot of researches. For example, the ballistic thermoelectric properties for the bended GNRs and the graphene with impurities have been investigated by the first-principles calculations and the quantum transport theory.[17,18]

For aGNR, the TB calculation results show that they may be conductors or semiconductors.[7,19] The first-principles results show that for the metal-type aGNR in the TB model, in fact, there is still a very small gap.[20,21] However, the TB method is still a brief and useful model. It employs the p_z orbital near the Fermi level to describe the electrical properties of GNR. The results basically agree with the first-principles calculations. In the GNR with a uniform stress, the TB model also gives roughly the same results as the first-principles calculation.[22,23]

For the uniform aGNR, an analytical solution was proposed.[24] In this solution, the transverse wave function of the ribbon was assumed to have a standing-wave form. Under this assumption, the electron states in a semi-infinite aGNR or in a uniform aGNR block were also studied.[25–27]

However, these analytical studies are only suitable for uniform nanoribbons. For inhomogeneous aGNR systems, to our knowledge, there has been no simple analytical expression and the energy band has to be obtained numerically. In this paper we develop a new one-dimensional (1D) analytical method which is suitable for the inhomogeneous aGNR systems. Within this 1D method, we calculate the energy band for aGNRs in the presence of various line defects or uniaxial strains. We also extend this method to the non-equilibrium Green's function (NEGF) theory for the transmission calculation. In the case of very large aGNR systems, our method can obtain accurate results without heavy computations because it only needs to deal with small matrices.

In the semi-infinite or block aGNR systems, the zigzag edges support some localized electron states, which are similar to the edge states in zGNR.[25–27] These states were also verified from the surface Green's function calculation in our previous work.[28] On the zigzag edges of bilayer graphene, the solutions of localized states were also proposed.[29] These local-

*Project supported by the Starting Foundation for the 'Hundred Talent Program' of Chongqing University, China (Grants No. 0233001104429).

†Corresponding author. E-mail: xiehangphy@cqu.edu.cn

© 2017 Chinese Physical Society and IOP Publishing Ltd

ized states are due to the zigzag edges or defects in graphene. In other materials such as silicon quantum dots and nanocrystals, people also found such local states. They are related to the dangling bonds, impurities or defects on curved surfaces with the energy in band gaps.[30–32]

In this paper we employ this 1D method to investigate these localized states in the aGNR or the boron-nitride nanoribbons with line defect. We obtain analytic solutions and the critical condition for these localized states in semi-infinite aGNRs. We also find some asymmetrical localized states in the boron-nitride nanoribbon with a line defect.

The rest of this paper is organized as follows. In Section 2, presented are the model and theory, including the 1D supercell method and its combination with the transfer matrix and the NEGF theory. In Section 3, the results, including the band structures and localized states in aGNR with line defects are given. The local states in the semi-infinite nanoribbon and the boron-nitride nanoribbon are also analyzed. Finally, some conclusion are drawn from the present study in Section 4.

2. Theory and models

2.1. 1D supercell method in aGNR system

For the simple aGNR as shown in Fig. 1(a), there are two types of carbon atoms (A and B) in one unit cell. In the tight binding model, the wavefunction can be written as the following form:[24]

$$\psi = C_A \sum_A \sum_{j=1}^{N} \mathrm{e}^{\mathrm{i}kx_A} \phi_A(j)\,|A\rangle + C_B \sum_B \sum_{j=1}^{N} \mathrm{e}^{\mathrm{i}kx_B} \phi_B(j)\,|B\rangle, \quad (1)$$

where $\phi_A(j)$ and $\phi_B(j)$ are the components for A and B sublattices with the index j in the y direction; $|A\rangle$ and $|B\rangle$ are the wave functions of p_z orbitals located in the A and B sublattices. C_A and C_B are superposition coefficients. The Bloch factors $\mathrm{e}^{\mathrm{i}kx_{A_i}}$ and $\mathrm{e}^{\mathrm{i}kx_{A_i}}$ are from the translational invariance in the horizontal direction. In the vertical direction, with the hard-wall boundary as shown in Fig. 1(a), we have

$$\begin{aligned} &\phi_A(0) = \phi_B(0) = 0, \\ &\phi_A(N+1) = \phi_B(N+1) = 0. \end{aligned} \quad (2)$$

Then the following standing-wave-formed wavefunction is obtained:

$$\phi_A(j) = \phi_B(j) = \sin\left(q_y j \frac{\sqrt{3}}{2} a\right). \quad (3)$$

With this form of wavefunction and the hard wall boundary condition, we have

$$q_y (N+1) \frac{\sqrt{3}}{2} a = p\pi, \quad (4)$$

where $p = 1, 2, \ldots, N$. Thus the wavefunction in the y direction can be written as

$$\phi_A(j) = \phi_B(j) = \sin\left(\frac{p\pi j}{N+1}\right). \quad (5)$$

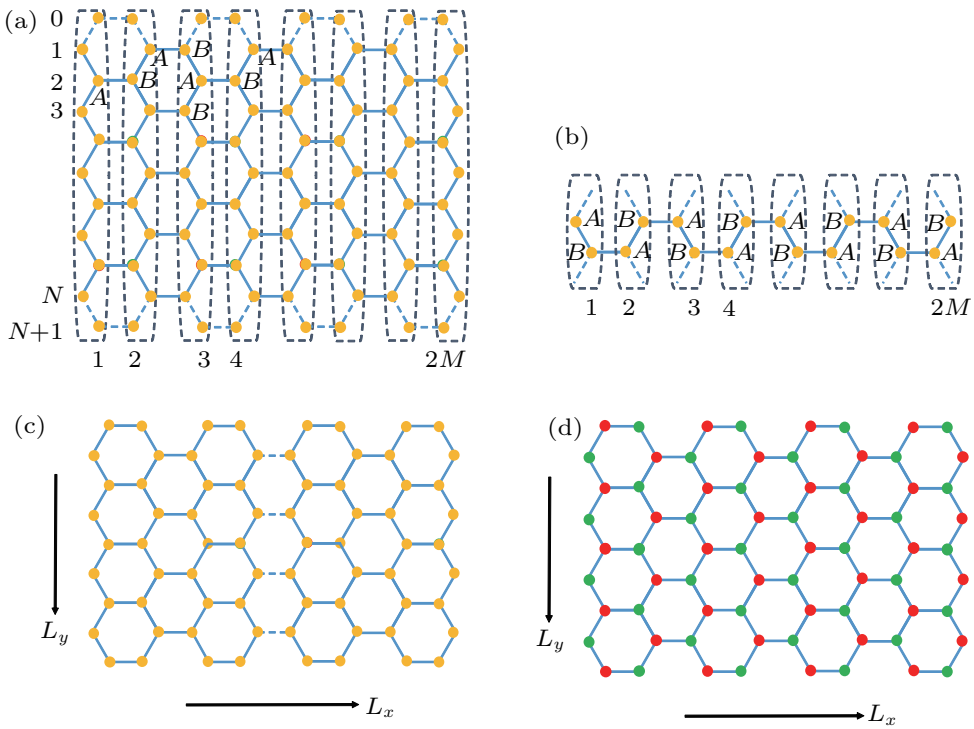


Fig. 1. (color online) Atomic structures for the armchair graphene or graphene-like nanoribbons. Panel (a) shows the simple aGNR, each unit cell contains N A- and B-carbon atoms. The dashed lines in the top/bottom region indicate the boundaries of the standing wave. Panel (b) shows the reduced 1D aGNR supercell with $2M$ sub-unit cells; panel (c) shows the aGNR supercell with an elongation-type line defect (indicated by the dash lines in the middle region); panel (d) shows the supercell of a boron-nitride nanoribbon. The boron atoms are green and the nitride atoms are red.

We substitute this form of the wavefunction into the Schrödinger equation with the tight-binding approximation and obtain the eigenvalue equation for the band calculation.[24] This standing-wave assumption of the wavefunction can reduce any uniform (in y direction) aGNR system into a 1D system. Figure 1(b) shows such a reduced 1D chain system. With this method, we can calculate some large system with a much less computation load.

Now we generalize this idea to the supercell system, including the supercell with some line defects. Usually the line defect in graphene consists of the periodically repeated one octagonal and two pentagonal rings in the y direction.[33,34] Here in this paper we only tune down some hopping parameters along the y direction, just as the bonds in the GNR are elongated by stress,[22,23] thereby presenting a simple 'line defect' (see Fig. 1(c)). This can maintain the hexagon topology in the aGNR for our 1D calculation. So the system is still uniform in the vertical direction, but the translation invariance in the horizontal direction is not satisfied due to the inhomogeneity. Furthermore, from Fig. 1(c) we see that the line defect destroys the six-member ring in one unit cell and the A-type atoms (or B-type atoms) in the original six-member ring are not equivalent to each other. So we have to separate the original unit cell into two new sub-unit cells (dash boxes in Fig. 1(b)). Also due to the broken translational symmetry, in the new model none of the superposition coefficients of A_n (and B_n) in different new sub-unit cells are not constant. These coefficients are involved in a set of equations for eigenvalue calculation.

We assume that the supercell system has N columns in the y direction and $2M$ sub-unit cells in the x direction. In the TB approximation, the wavefunction can be written as

$$|\psi\rangle = \sum_{n=1}^{2M}\left[\sum_{j=1}^{N}\phi_A(j)\cdot A_n|A\rangle + \sum_{j=1}^{N}\phi_B(j)\cdot B_n|B\rangle\right], \tag{6}$$

where $\phi_A(j)$ and $\phi_B(j)$ are the components of A-type atom and B-type atom in the j-th column of the sub-unit cell (see Eq. (5)). A_n and B_n denote the coefficient components of A-type atom and B-type atom in the horizontal direction. Under the TB approximation, the Hamiltonian is written as

$$H = \sum_i \varepsilon_i|i\rangle\langle i| + \sum_{\langle i,j\rangle} t_{i,j}|i\rangle\langle j|, \tag{7}$$

where $\langle i,j\rangle$ denotes the nearest neighbors. If we choose $\varepsilon_i = 0$ and $t_{i,j} = t$, and substitute Eqs. (6) and (7) into the Schrödinger equation, then we will have the following equation for the A-type atoms in an aGNR supercell,

$$\begin{aligned} &E\phi_A(j)A_n - t\phi_B(j)B_{n+1} \\ &-t\phi_B(j+1)B_n - t\phi_B(j-1)B_n = 0. \end{aligned} \tag{8}$$

Similarly, we have the following equation for the B-type atoms in an aGNR supercell

$$\begin{aligned} &E\phi_B(j)B_n - t\phi_A(j)A_{n-1} \\ &-t\phi_A(j+1)A_n - t\phi_A(j-1)A_n = 0. \end{aligned} \tag{9}$$

Substituting Eq. (5) into Eqs. (8) and (9), and with some derivations, we have

$$EA_n - tB_{n+1} - 2t\cos\left(\frac{p\pi}{N+1}\right)B_n = 0, \tag{10a}$$

$$EB_n - tA_{n-1} - 2t\cos\left(\frac{p\pi}{N+1}\right)A_n = 0. \tag{10b}$$

We see that the two equations above are j-independent. This means that the system is transformed into the 1D form. Then we employ the Bloch boundary condition

$$B_{2M+1} = \mathrm{e}^{\mathrm{i}k2aM}B_1, \tag{11a}$$

$$A_0 = \mathrm{e}^{-\mathrm{i}k2aM}A_{2M}. \tag{11b}$$

Substituting this Bloch boundary condition into Eq. (10), we obtain the eigenvalue matrix equation which involves the Bloch wave vector k. For an aGNR supercell with $2M$ unit cells in the x direction, there are $4M$ unknowns (A_n and B_n). For each matrix equation, we find that the number of p values (Eq. (5)) that can be chosen is $N/2$, which corresponds to the number of the standing-wave modes in the y direction (which will be discussed in more detail later). So the total number of eigenvalues is $2MN$, which exactly equals the number of energy bands in the common TB method.

The equations above are for the uniform (in the x direction) aGNR supercell. For the supercell with a line defect, we assume that the defect only changes the hopping integral t as in the strained GNR,[22,23] equations (10a) and (10b) are modified into

$$EA_n - t_n^{A,1}B_{n+1} - 2t_n^{A,2}\cos\left(\frac{p\pi}{N+1}\right)B_n = 0, \tag{12a}$$

$$EB_n - t_n^{B,1}A_{n-1} - 2t_n^{B,2}\cos\left(\frac{p\pi}{N+1}\right)A_n = 0, \tag{12b}$$

where $t_n^{A,1}$ and $t_n^{A,2}$ correspond to the hopping integrals from the A-type atoms, with $t_n^{A,1}$ being the hopping integral from A-type atom to the forward horizontal B-type atom, and $t_n^{A,2}$ being the hopping integral from A-type atom to the top (bottom)-left B-type atoms; $t_n^{B,1}$ and $t_n^{B,2}$ are defined similarly to those in Fig. 1(b). We assume that the line defect only changes the hopping integrals in the horizontal direction. It is easy to see that $t_{n-1}^{A,1} = t_n^{B,1}$ and $t_n^{A,2} = t_n^{B,2}$.

With the approach above, we set up a new one-dimensional model formulism for the band structure calculation of an aGNR supercell system.

2.2. Calculations for the localized state in a semi-infinite aGNR

Here we consider a simple semi-infinite aGNR as shown in Fig. 1(a). According to the theory we generalized before, equations (10a) and (10b) also hold except the equation in the boundary sub-unit, which is modified into

$$EB_1 - 2t\cos\left(\frac{p\pi}{N+1}\right)A_1 = 0. \tag{13}$$

From Eqs. (10a) and (10b), we obtain a transfer matrix equation

$$\begin{aligned}\begin{pmatrix} B_{n+1} \\ A_{n+1} \end{pmatrix} &= \boldsymbol{T}\begin{pmatrix} B_n \\ A_n \end{pmatrix} \\ &= \begin{pmatrix} -\tau t^{-1} & Et^{-1} \\ -Et^{-1} & t^{-1}E^2\tau^{-1} - t\tau^{-1} \end{pmatrix}\begin{pmatrix} B_n \\ A_n \end{pmatrix}, \end{aligned} \tag{14}$$

where $\tau = 2t\cos\left(\frac{p\pi}{N+1}\right)$. To solve the semi-infinite problem by this transfer matrix method, we calculate the eigenvalues λ_1 and λ_2, and the corresponding eigenvectors $[U_{11}, U_{21}]^{\mathrm{T}}$ and $[U_{12}, U_{22}]^{\mathrm{T}}$ of $\boldsymbol{T}$. The two eigenvalues satisfy the condition $\lambda_1\lambda_2 = 1$. To obtain a solution of localized (decaying) state, the eigenvalues must be real. Assume $\lambda_1 < 1$ and $\lambda_2 > 1$, then we will have

$$\begin{pmatrix} B_{n+1} \\ A_{n+1} \end{pmatrix} = \begin{pmatrix} U_{11} & U_{12} \\ U_{21} & U_{22} \end{pmatrix}^{-1}\begin{pmatrix} \lambda_1 & 0 \\ 0 & \lambda_2 \end{pmatrix}\begin{pmatrix} U_{11} & U_{12} \\ U_{21} & U_{22} \end{pmatrix}\begin{pmatrix} B_n \\ A_n \end{pmatrix}.$$

Iterating the formula above, we obtain the following result:

$$\begin{aligned}\begin{pmatrix} B_{n+1} \\ A_{n+1} \end{pmatrix} &= \begin{pmatrix} U_{11} & U_{12} \\ U_{21} & U_{22} \end{pmatrix}^{-1}\begin{pmatrix} \lambda_1^n & 0 \\ 0 & \lambda_2^n \end{pmatrix} \\ &\times \begin{pmatrix} U_{11} & U_{12} \\ U_{21} & U_{22} \end{pmatrix}\begin{pmatrix} B_1 \\ A_1 \end{pmatrix}. \end{aligned} \tag{15}$$

Since we assume $\lambda_2 > 1$, to avoid the divergence of the wavefunction, the following condition is required:

$$U_{21}B_1 + U_{22}A_1 = 0. \tag{16}$$

Combining the boundary equation (Eq. (13)) and Eq. (16), we have

$$\begin{pmatrix} U_{21} & U_{22} \\ E & -2t\cos\left(\frac{p\pi}{N+1}\right) \end{pmatrix}\begin{pmatrix} B_1 \\ A_1 \end{pmatrix} = \boldsymbol{D}\begin{pmatrix} B_1 \\ A_1 \end{pmatrix} = 0.$$

We see that $\det\boldsymbol{D} = 0$ is a sufficient condition for the existence of a localized state. Our calculation indicates that such a condition can be satisfied only with $E = 0$. Such a conclusion is consistent with the Jiang *et al.*'s result.[25] When $E = 0$, we can easily obtain the localized state solution from Eqs. (13) and (14) as follows:

$$A_n = 0, \tag{17a}$$

$$B_n = \left(-2\cos\left(\frac{p\pi}{N+1}\right)\right)^{n-1}B_1. \tag{17b}$$

For a convergent solution, it is apparent that p satisfies the condition

$$2\cos\left(\frac{p\pi}{N+1}\right) < 1,$$

or

$$p > \frac{N+1}{3}. \tag{18}$$

We find that this local state also exists in finite-sized graphene nanoribbons (or graphene quantum dots).[35] In Ref. [35],

$$\frac{2p\pi}{(N+1)a_0} - \frac{2\pi}{3a_0} > \frac{1}{L_y}$$

is the sufficient condition for the existence of a local state for finite-sized graphene nanoribbons. As for a semi-infinite aGNR $L_y \to \infty$, we have $p > (N+1)/3$. This conclusion is consistent with Eq. (18). It is easy to understand that for the energy band beside the Dirac point, $E \propto \sqrt{k_x^2 + k_y^2}$. If k_x is a pure imaginary number, k_y must have a larger absolute value than that of k_x.

Finally, if A-type atom and B-type atom are different as shown in Fig. 1(d) in an armchair boron–nitride nanoribbon,[36] equations (10a), (10b), and (13) are modified, respectively, into

$$(E - \varepsilon_B)B_1 - 2t\cos\left(\frac{p\pi}{N+1}\right)A_1 = 0, \tag{19a}$$

$$(E - \varepsilon_A)A_n - 2t\cos\left(\frac{p\pi}{N+1}\right)B_n - tB_{n+1} = 0, \tag{19b}$$

$$(E - \varepsilon_B)B_{n+1} - 2t\cos\left(\frac{p\pi}{N+1}\right)A_{n+1} - tA_n = 0, \tag{19c}$$

where ε_A and ε_B are the on-site energies of A-type atom and B-type atom. When $E = \varepsilon_B$, we can obtain a similar localized state.

2.3. Transmission calculation in aGNR system with the NEGF theory

We also use this 1D model to calculate the transmission spectrum or local density of states (LDOS) for armchair graphene-like nanoribbons with the NEGF theory.[37] The system has to be uniform in the y direction for the feasibility of our 1D method. From Eqs. (10a and (10b), we can obtain the surface Green's function of a semi-infinite 1D aGNR by the Dyson's equation,

$$g_p^{\mathrm{r}} = \frac{E^2 + t^2 - \tau^2 + \sqrt{(E^2 + t^2 - \tau^2)^2 - 4E^2t^2}}{2t^2E}, \tag{20}$$

where $\tau = 2t\cos\left(\frac{p\pi}{N+1}\right)$ and $p = 1, 2, 3, \ldots N/2$. We see that there exists a bound state when $E = 0$, which is self-consistent with our previous conclusion. With the NEGF theory, we have

$$\left(E_p\boldsymbol{I} - \boldsymbol{H}_p - \Sigma_p^{\mathrm{r}}\right)\boldsymbol{G}_p^{\mathrm{r}} = \boldsymbol{I}, \tag{21}$$

$$\Sigma^{\mathrm{r}}_{\alpha,p} = \boldsymbol{h}_{D\alpha,p} g^{\mathrm{r}}_{\alpha,p} \boldsymbol{h}_{\alpha D,p}, \tag{22}$$

where $\boldsymbol{I}$ is a unitary matrix with the dimension of the 1D model device; $\Sigma^{\mathrm{r}}_{\alpha,p} = \Sigma^{\mathrm{r}}_{\mathrm{L},p} + \Sigma^{\mathrm{r}}_{\mathrm{R},p}$ is the retarded self-energy with the mode p, which is given by the coupling Hamiltonians and the surface Green's function of mode p; $g^{\mathrm{r}}_{\alpha,p}$ is given by Eq. (20). ($\alpha = \mathrm{L},\mathrm{R}$, which means the left or right lead.) The imaginary part of $\boldsymbol{G}^{\mathrm{r}}_{i,i,p}$ gives the local density of states (LDOS) of mode p,

$$\rho_{i,p}(E) = -\frac{1}{\pi} \mathrm{Im}[G^{\mathrm{r}}_{i,i,p}(E)]. \tag{23}$$

And the transmission coefficient of mode p can be calculated from the NEGF theory[29]

$$T_p = \mathrm{tr}\left[\boldsymbol{G}^{\mathrm{r}}_p \Gamma_{\mathrm{L},p} \boldsymbol{G}^{\mathrm{a}}_p \Gamma_{\mathrm{R},p}\right], \tag{24}$$

where $\Gamma_{\alpha,p} = \mathrm{i}\left[\Sigma^{\mathrm{r}}_{\alpha,p} - \Sigma^{\mathrm{a}}_{\alpha,p}\right]$ and $\boldsymbol{G}^{\mathrm{a}}_p = \left[\boldsymbol{G}^{\mathrm{r}}_p\right]^{\dagger}$. We find that the total transmission coefficient is the sum of transmission coefficients of all modes (p ranges from 1 to $N/2$). With this method, we can avoid heavy matrix computations in calculating the transmission coefficient of very large GNR systems.

3. Results and discussion

3.1. Band and transmission calculations for simple aGNRs

Firstly, we use Eq. (10) to calculate a simple aGNR for a benchmark. It is a supercell with $M = 2$. The hopping integral of the aGNR is chosen as $t = -2.7$ eV, which agrees well with the results from the first principle calculations.[12] For the widths with $N = 6$ and $N = 8$, we give the band structures and transmission spectra in Figs. 2(a)–2(d). The band structures agree well with the results in Ref. [24], and the transmission spectra are also consistent with those of the band structures.

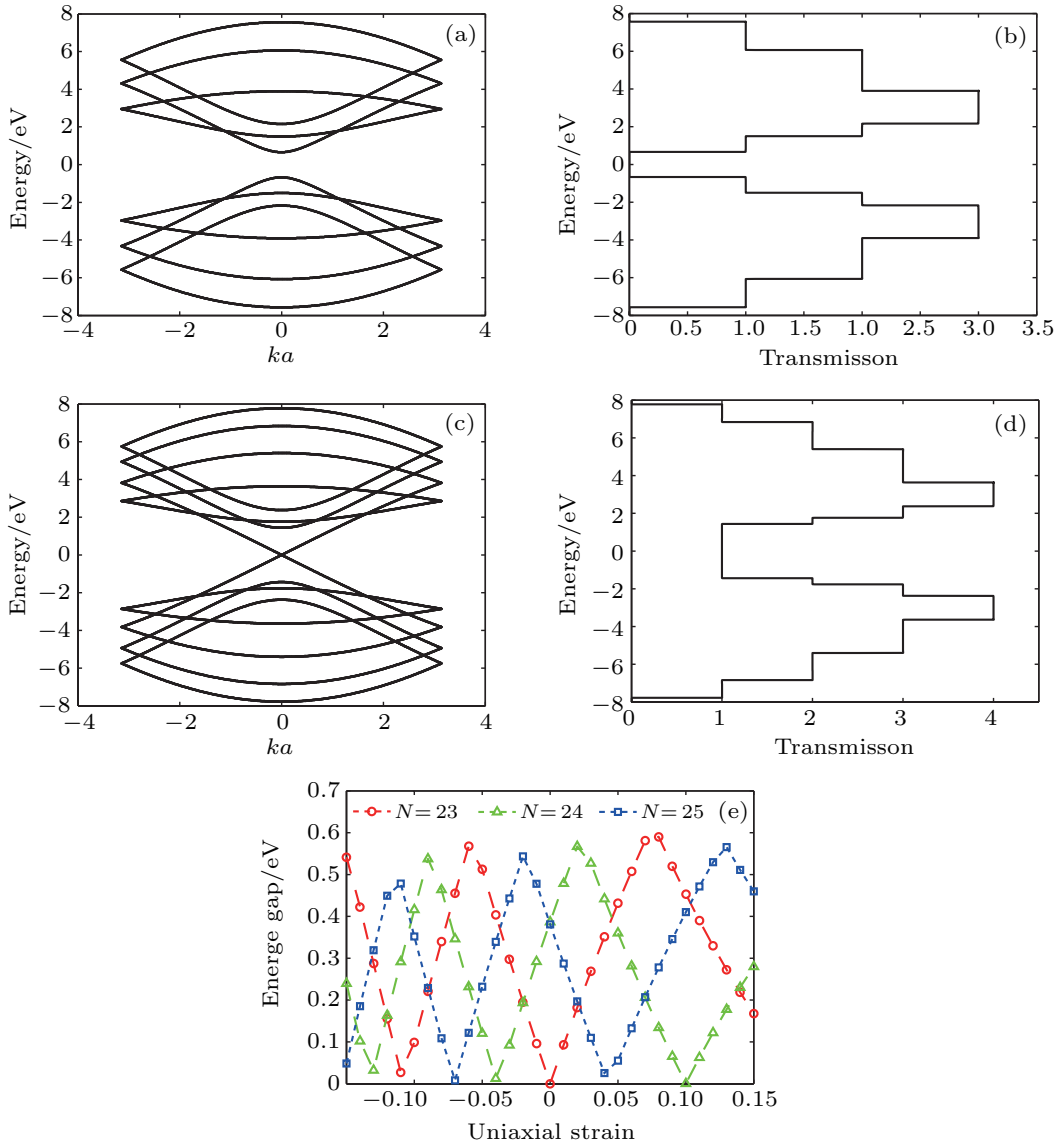


Fig. 2. (color online) Band structures, transmission spectra and energy gaps of simple aGNRs ($2M = 2$). Panels (a) and (b) show the band structure and transmission of a simple aGNR with $N = 6$, panels (c) and (d) the band structure and transmission of a simple aGNR with $N = 8$, panel (e) displays the band gaps of aGNRs with uniaxial strain σ in x direction. In panels (a) and (c), a is the period of the supercell and $a = 3a_0$, where a_0 is the lattice constant of aGNR.

Our method can also calculate the band in aGNR with uniaxial strain.[23] As the method developed in Refs. [22] and [23], the three bond vectors in the aGNR are changed with the uniaxial strain σ in the x direction as $r_{ix} \to (1+\sigma)r_{ix}$; $r_{iy} \to (1-\nu\sigma)r_{iy}$, where $\nu = 0.165$ is the Poisson ratio.[23] The hopping integrals are scaled by the factor $\xi = (r_0/r)^2$, where r_0 is the unstrained bond length and r is the bond length with strain. With some derivations, the new hopping integrals in Eq. (12) are obtained to be $t_n^{A,1} = t_n^{B,1} = t_0\left(1-2\sigma+3\sigma^2\right)$ and

$$t_n^{A,2} = t_n^{B,2} = \left[\frac{1}{2}\left(1+\sigma^2\right)^2 + \frac{3}{2}(1-\nu\sigma)^2\right]^{-1} \approx t_0\left(1-\frac{1}{2}\sigma+\frac{3}{2}\nu\sigma\right).$$

We choose the supercell sizes with $2M = 2$ and $N = 23$, 24, 25, which correspond to the cases of $N+1 = 3q$, $3q+1$, and $3q+2$.[20] We calculate the band gaps in aGNR with different strains as shown in Fig. 2(e). We find that the band gap periodically changes with strain. Our results agree well with the results from the perturbation theory calculations.[23] And our results come back to the unstrained cases[20] when $\sigma = 0$.

3.2. Band structures of aGNR with a line defect

With this supercell method, we now calculate the band structure of the aGNR supercell with a line defect as shown in Fig. 1(c). We choose the hopping integrals at the defect positions: $t_{n-1}^{A,1} = t_n^{B,1} = -0.5$ eV. Other hopping integrals are all set to be the value of -2.7 eV. With Eq. (12) and the boundary condition (Eq. (11)), we set up a matrix equation for the eigenvalue calculation. The calculated band structures are shown in Fig. 3 below.

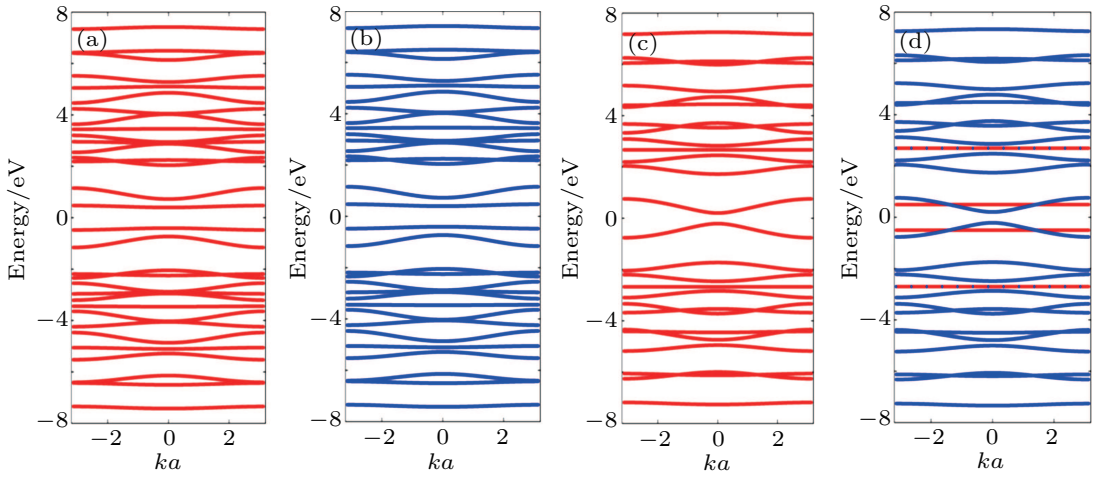


Fig. 3. (color online) Band results from ((a) and (c)) the common 2D-TB method (red lines) and ((b) and (d)) our 1D supercell method (blue lines) for aGNR supercell with a line defect for the cases of ((a) and (b)) $N = 8$, $2M = 4$, and ((c) and (d)) $N = 7$, $2M = 4$. In panel (d) the red lines denote the bands which need deducing.

Figure 3(a) and 3(b) are for the supercell with the size $N = 8$, $2M = 4$. As stated before, we choose $N/2$ p values for the eigenvalue calculations. In each eigenvalue matrix, there are $4M$ eigenvalues. So the total number of the bands for this system is 32 $(2M \times N)$, which is the total number of the atoms in the aGNR supercell.

Now we study another case where the supercell has the size $N = 7$, $2M = 4$. In this case, N is an odd number. We find that if we chose the value of $(N+1)/2$ or $(N-1)/2$ p, the total number of bands is $2(N+1)M$ or $2(N-1)M$, which is not equal to the number of bands in the 2D-TB model $(2MN)$.

Here we give a detailed analysis of this discrepancy. As we stated previously, each p value corresponds to a type of standing wave in the y direction in the 1D model. In a simple aGNR, A-type and B-type atoms are equivalent to each other, so p value can be chosen from 1 to N.[24] Here in our supercell (with line defects) case, A-type and B-type atoms are not equivalent to each other. There are $(N-1)/2$ (or $(N+1)/2$) A-type atoms and $(N+1)/2$ (or $(N-1)/2$) B-type atoms in each separated unit cell. So they have different numbers of the corresponding standing waves. In this method, for each $4M \times 4M$ matrix equation we have to choose a value of $(N+1)/2$ p. Thus we obtain a total number of $2M \times (N+1)$ bands in the calculation. Then we have to artificially take out $2M$ bands for A-type atoms with $p = (N+1)/2$. The final number of the left bands is $2M \times N$, which coincides with the result of the 2D-TB model.

In Fig. 3(c) we obtain $7 \times 4 = 28$ bands from the 2D-TB calculation. From the 1D-supercell calculation, the total number of bands with a value of $(N+1)/2$ p is $4 \times 8 = 32$ as shown in the blue lines in Fig. 3(d). Then we deduct $2 \times M = 4$ bands (red lines at $+/-0.5$ eV and $+/-2.7$ eV) for $p = (N+1)/2$ (the left flat bands at $+/-2.7$ eV are 2-fold degenerate), and the left bands are exactly the same as those in Fig. 3(c).

We notice that this 1D-supercell method gives the same band result as the 2D-TB method, only if the aGNR supercell is uniform in the y direction. For a very large system our 1D-supercell method has a much small computation load, since it only needs to solve $4M^* \times 4M$ eigenvalue matrices, instead of as large as $(2M \times N) \times (2M \times N)$ eigenvalue matrix.

3.3. Localized states in aGNR supercells

Now we begin to analyze the localized states in these aGNRs. The edge states are well known in the zigzag GNR. Here we find that in the armchair GNR, if there is some line defect, there also exist such edge states, which are localized near the line defect. These localized states result from the zigzag edge structures, and they have been discussed in the literature before.[27,37]

We calculate an aGNR supercell ($N = 23$, $2M = 16$) with a line defect on the supercell boundaries. The hopping integrals in the defect are set to be $t_1 = t_{n-1}^{A,1} = t_n^{B,1} = -0.5$ eV. Figure 4(a) draws the band structure near the Fermi level. The numbers in the band figure denote the p values. Figures 4(b) and 4(c) show the electron density distribution for the band which is the closest to the Fermi level ($p = 9$, $k = 0$) by the 2D-TB method. We also calculate the electron distribution for $p = 9$ with the k values averaged in the first Brillouin zone. The result is very similar to that in the $k = 0$ case. We see that the electron is localized near the line defect in the supercell, so that it is a defect state. In the y direction, there are 3 peaks on the edge. From our method, those 3 peaks may be explained by the standing-wave formula. In the y direction, the electron density behaves as a function of $\sin^2\left(\frac{p\pi j}{N+1}\right)$. So different p indices correspond to different peak patterns in the lateral direction. We believe that the STM experiment can detect these defect edge states as well.

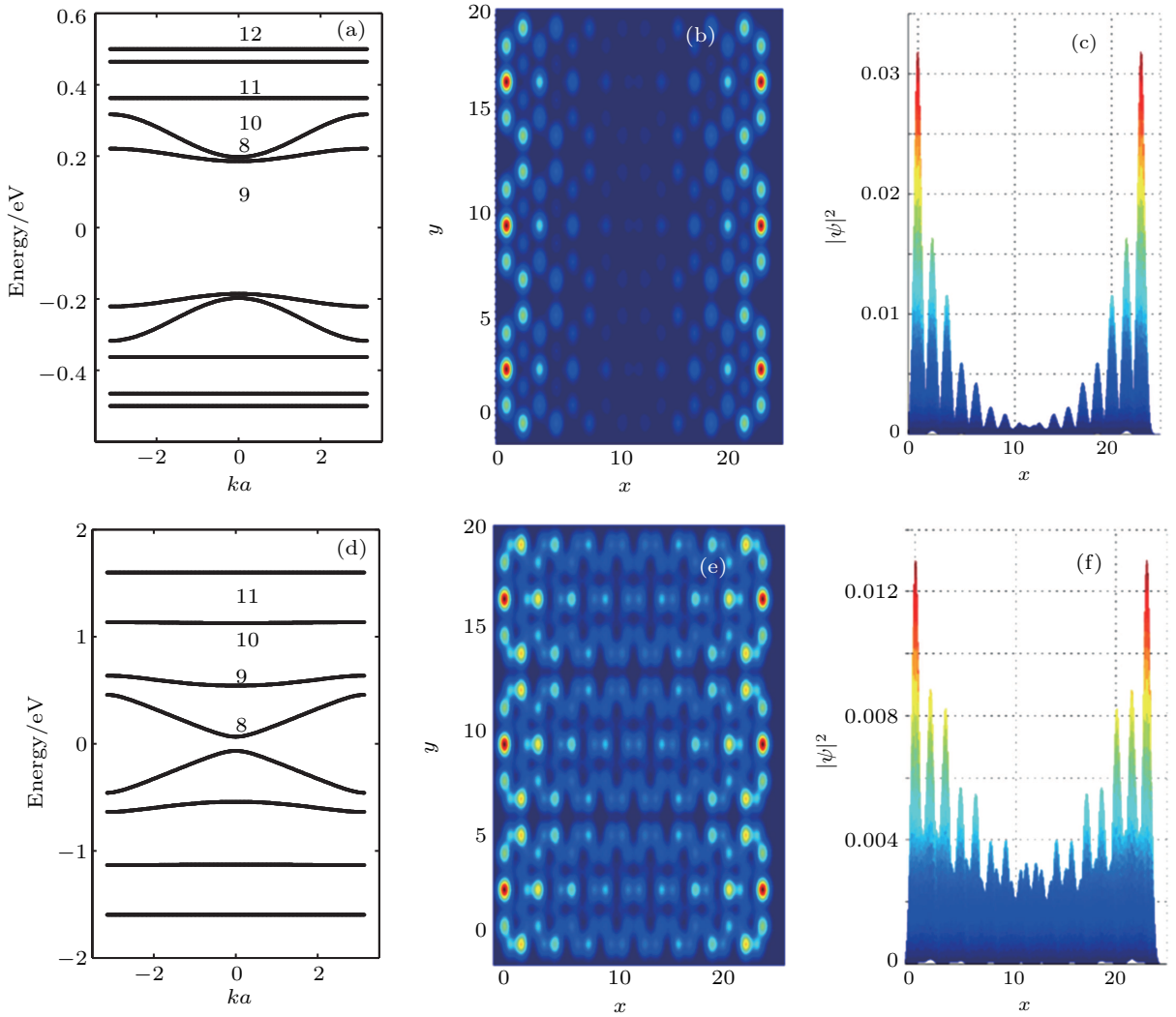


Fig. 4. (color online) Band structures and the electron density distributions for the edge state in a GNR supercell ($N = 23$, $2M = 16$) with line defect. Panel (a) shows the bands near the Fermi level with a strong defect ($t_1 = -0.5$ eV). The numbers indicate the p values of the 1D-supercell model; Panels (b) and (c) display the electron density distribution of the edge state for $p = 9$ band with $k = 0$ and $t_1 = -0.5$ eV. Panel (d) exhibits bands near the Fermi level with a weak defect ($t_1 = -1.8$ eV). Panels (e) and (f) indicate the electron density distribution of the edge state for $p = 9$ band with $k = 0$ and $t_1 = -1.8$ eV. In the density distribution figures, panels (b) and (e) are the overhead views; panels (c) and (f) are the side views of the 3D plot.

Then we tune the hopping integral t_1 to a lower energy (-1.8 eV), the energy band with $p = 8$ becomes lower than the band with $p = 9$. And the electron density distribution with $p = 9$ is plotted as well (see Figs. 4(d)–4(f)). We see with the lower t_1, the edge state becomes more delocalized. In other words, when the line defect effect becomes smaller, the wave localization also becomes weaker. We also observe that the band for $p = 9$ becomes flatter in the strong-defect case than in the weak-defect case by comparing their average slopes in the Brillouin zone. This means that the defect can reduce the group velocity for the state near the Fermi level. In the limit of t_1 equal to t_0 (-2.7 eV), the edge state will be replaced by a uniform state in the x direction.

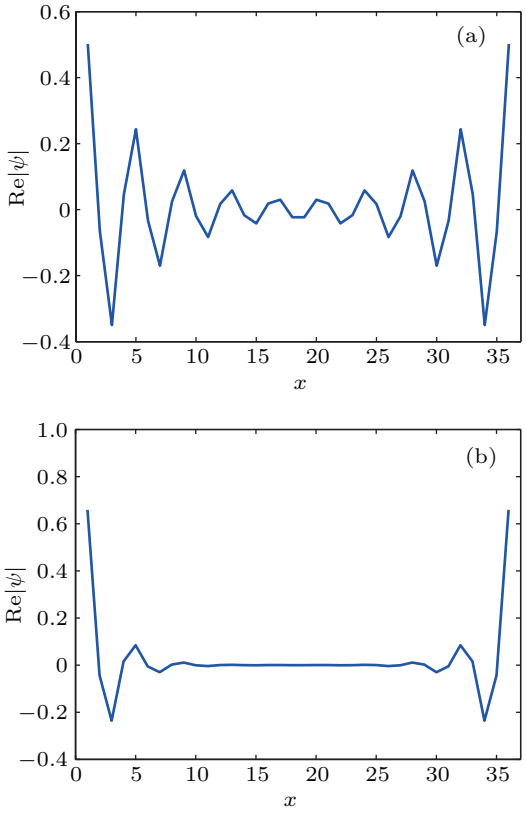


Fig. 5. (color online) Localized states in a long aGNR supercell with the isolate line defect ($t_1 = 0$). The size of the supercell is set to be $N = 17$, $2M = 36$. Panel (a) is for the wavefunction of the 1D-supercell model with $p = 7$, panel (b) the wavefunction of the 1D-supercell model with $p = 8$.

From Subsection 2.2, we see that in a semi-infinite aGNR the localized state exists only when $p > (N+1)/3$. We find that this condition also holds for the possible local states in the defect-involved aGNR supercells, if the p value is chosen to be close to the Fermi level, and the hopping integral t_1 is set to be about zero, like an isolate system. Figures 5(a) and 5(b) show an example ($N = 17$, $2M = 36$) for the wavefunction (real part) in the x direction by the 1D-supercell method. They correspond to the side views of the 3D electron density distribution. The defects are positioned on the left and right sides of the supercell. We see that for the local edge states, p value should satisfy $(N+1)/3 < p \leq (N+1)/2$. The upper bound come from the standing wave condition as stated before. In this case there are three available p values ($p = 7, 8, 9$).

In Figs. 5(a) and 5(b) we see that the wavefunctions are localized near the two boundaries (line defects). From Eq. (17b) we know that a large p value corresponds to a stronger decaying mode. In Fig. 5 we see that the wavefunction with $p = 8$ has a more localized behavior than that with $p = 7$ as expected. We also check that when $p \leq 6$, there are no local states in the supercell system. The physical reason is that the mode with a large p value corresponds to a high-lying lateral standing-wave mode and thus a small decaying wavevector. This is similar to the scenario of the evanescent mode of 2D-electron gas in a waveguide.

3.4. Localized states in the semi-infinite aGNR

Now we consider the localized state near the edge of a semi-infinite aGNR. As discussed in Subsection 2.2, the local state exists only at $E = 0$ and $A_n = 0$. We assume that $B_n = 1$ and utilize the iteration relation in Eq. (17b) to calculate B_n ($n > 1$) for these local states in a semi-infinite aGNR. Then we use Eq. (5) to recover the 1D result into the 2D case. Figure 6 gives an example for the localized state in a semi-infinite aGNR with the width $N = 23$ and the standing-wave number $p = 9$.

From Fig. 6 we see that this state is very similar to the local state in the aGNR supercell with a strong line defect.

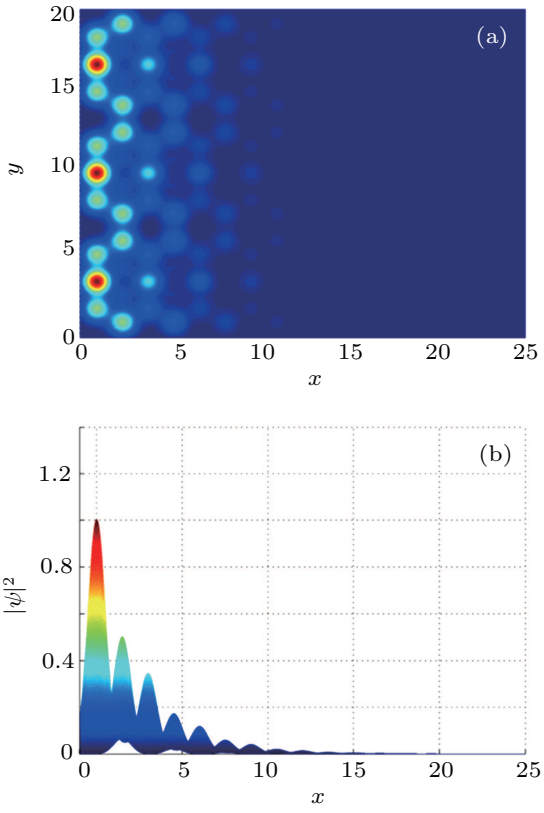


Fig. 6. (color online) Electron density distribution of the localized state in a semi-infinite aGNR ($N = 23$, $p = 9$). Panel (a) shows the overhead view and panel (b) the side view of the 3D plot.

This is reasonable since a very long supercell with a strong line defect ($t_1 = 0$) can be regarded as two combined semi-infinite systems. In the y direction, the peak patterns are also agreeable with the stand-wave formula $\sin^2(p\pi j/(N+1))$ as stated in Fig. 4 before.

3.5. Localized states in the armchair boron-nitride nanoribbon

Boron-nitride (BN) nanoribbon is very similar to the graphene nanoribbon, except that in the boron–nitride nanoribbon, A-type and B-type atoms are different (Fig. 1(d)). We can also use the method we introduced in Section 2 to calculate the energy band and localized state. The parameters of the TB calculation are listed in Table 1.[36]

Table 1. Tight binding parameters for the boron-nitride nanoribbon.

TB parameter	Value/eV
ε_N	–1.45
ε_B	3.2
t_{B-N}	–2.45

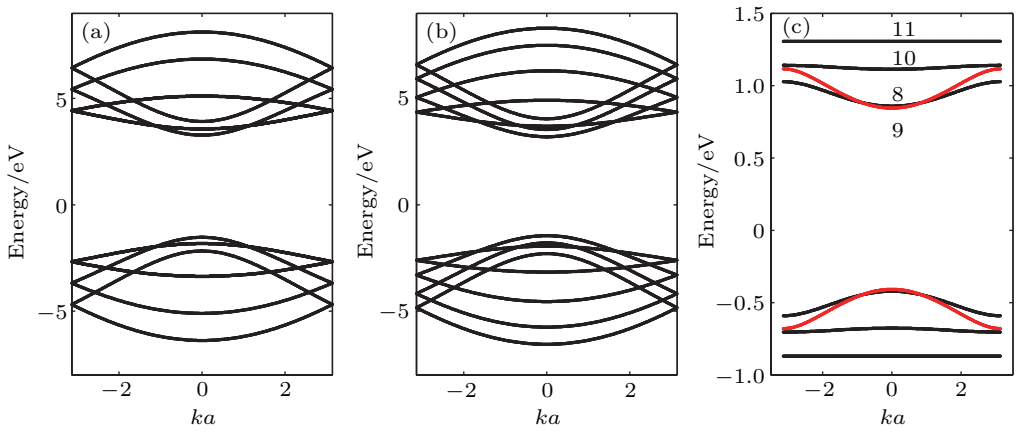


Fig. 7. (color online) Band structures of armchair BN nanoribbons from the 1D-supercell method for the cases of (a) $N = 6$, $2M = 2$; (b) $N = 8$, $2M = 2$; (c) $N = 23$, $2M = 16$, the red lines are for $p = 8$. In this figure, a is the period of the supercell.

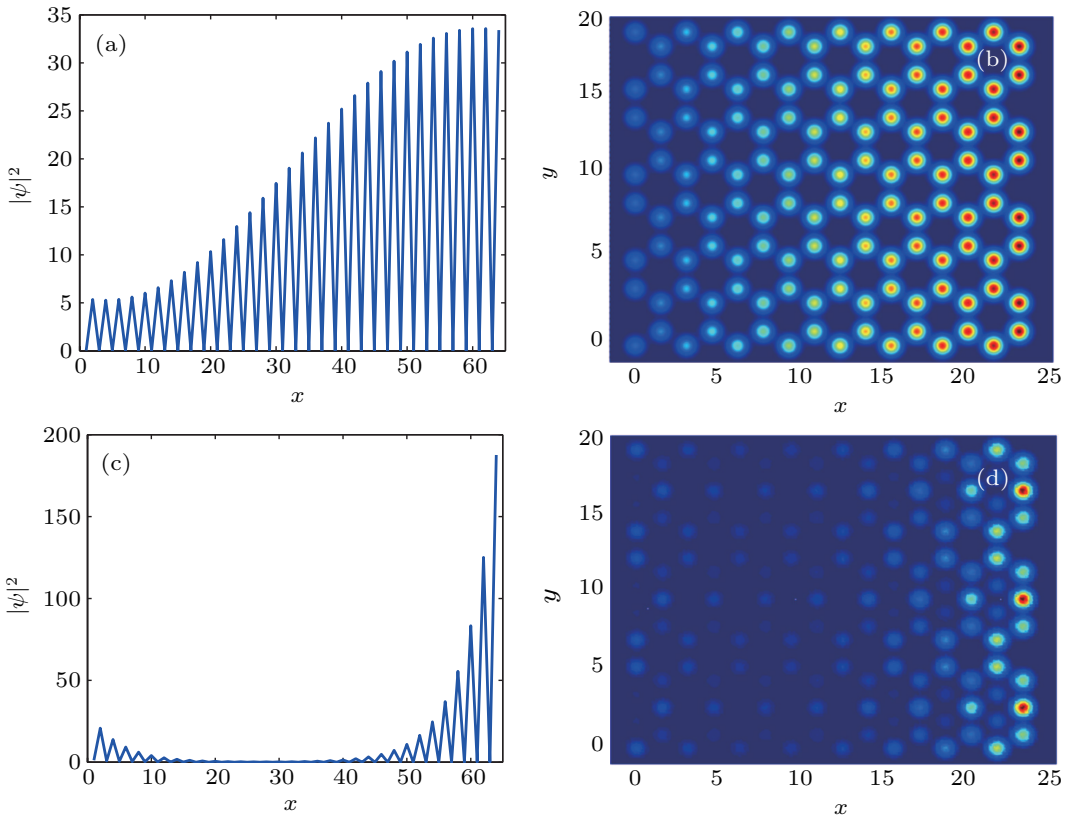


Fig. 8. (color online) Localized states in an armchair BN nanoribbon supercell with the line defect ($t_1 = -1.0$ eV). The size of the supercell is set to be $N = 23$, $2M = 16$. Panel (a) shows the wavefunction of the localized state with $p = 8$ in the 1D-supercell model, panel (b) the electron density distribution of the localized state with $p = 8$ in the 2D-TB model, panel (c) the wavefunction of the localized state with $p = 9$ in the 1D-supercell model, and panel (d) the electron density distribution of the localized state with $p = 9$ in the 2D-TB model.

We first calculate the energy bands of two single-column armchair BN nanoribbons with the geometric sizes: ($2M = 2$, $N = 6$) and ($2M = 2$, $N = 8$) as shown in Figs. 7(a) and 7(b), respectively. Because of breaking the symmetries of A-type atom and B-type atom, a large band gap is open compared with the band of aGNR (see Figs. 2(a) and 2(c)). For $N = 8$, the graphene nanoribbon is gapless since it is $3m+2$ type,[20,24] while the BN nanoribbon has a large gap due to breaking the symmetries of ε_N and ε_B.

Then we choose an armchair BN nanoribbon supercell with a line defect and the size parameters $N = 23$, $2M = 16$ (see Fig. 1(d)). The hopping integrals at the defect positions are set to be $t_1 = t_{n-1}^{A,1} = t_n^{B,1} = -1.0$ eV. We use our 1D-supercell method to calculate the bands (Fig. 7(c)) and two local states for the bands near the Fermi level with $p = 8$ and 9 (Fig. 8, with $k = 0$ in the reciprocal space). This 1D-supercell method gives the same results as those from the 2D-TB method. The local state is asymmetric because the A-type and B-type atoms are different.

In Figs. 8(a) and 8(b), it seems that the wavefunction decays only from the right to the left. In fact, it also decays from the left side to the right side as seen apparently in Figs. 8(c) and 8(d). The decaying trend from the left side is hidden by another trend which decays from the right side. In this supercell the nitrogen atoms are on the right boundary and the boron atoms are on the left boundary. As $\varepsilon_N < \varepsilon_B$ (Table 1), we find that for the band besides the Fermi level, the electron density near the nitrogen-atom boundary (right) is larger since these atoms have a lower energy. The electron densities from both boundaries all decay towards the inner region of the supercell. Comparing Fig. 8(a) with Fig. 8(c), it is easy to see that the decaying trend with $p = 9$ is stronger than that with $p = 8$. We may explain this by regarding the BN nanoribbon unit with a line defect as a quasi-semi-infinite ribbon. From Eq. (17(b)), we see that the decaying trend is larger with a large p value. It is also observed in Fig. 7(c) that the band with $p = 9$ is flatter than the band with $p = 8$, which indicates a smaller group velocity for the first band.

4. Conclusions

In this paper we develop a new 1D method for the armchair GNR-like systems, including the supercells with line defects and uniaxial strains. Our method gives the same results as the 2D-TB method. However, our method may save a lot of computation load for very large systems. By this method we investigate the properties of many localized defect edge states in these systems. A condition for these localized states to exist in the semi-infinite aGNR is derived as $p > (N+1)/3$. We find that this condition is also a criterion for the localized states in the aGNR supercells with a strong line defect (a small hopping integral near the defect).

We also study the BN nanoribbon supercell. We find that there exists some asymmetric localized state in these BN nanoribbons. For all of these defect states, the localization degree depends on two factors: the defect intensity (the hopping integral) and the lateral standing-wave index (p value).

This method is suitable for the band calculation of the armchair-like 2D materials. We will apply it to these materials in the future study.

Acknowledgement

The authors are grateful to Dr. Rui Wang of Chongqing University for the help with computer service.

References

[1] Novoselov K S, Geim A K, Morozov S V, Jiang D, Zhang Y, Dubonos S V, Grigorieva I V and Firsov A A 2004 *Science* **306** 666
[2] Castro Neto A H, Guinea F, Peres N M R, Novoselov K S and Geim A K 2009 *Rev. Mod. Phys.* **81** 109
[3] Dutta S and Pati S K 2010 *J. Mater. Chem.* **20** 8207
[4] Beenakker C W J 2008 *Rev. Mod. Phys.* **80** 1337
[5] Allain P E and Fuchs J N 2011 *Eur. Phys. J. B* **83** 301
[6] Wu X S, Hu Y K, Ruan M, Madiomanana N K, Hankinson J, Sprinkle M, Berger C and De Heer W A 2009 *Appl. Phys. Lett.* **95** 223108
[7] Nakada K, Fujita M, Dresselhaus G and Dresselhaus M S 1996 *Phys. Rev. B* **54** 17954
[8] Fujita M, Wakabayashi K, Nakada K and Kusakabe K 1996 *J. Phys. Soc. Jpn.* **65** 1920
[9] Yazyev O V 2010 *Rep. Prog. Phys.* **73** 056501
[10] Pisani L, Chan J A, Montanari B and Harrison N M 2007 *Phys. Rev. B* **75** 064418
[11] Barone V, Hod O and Scuseria G E 2006 *Nano Lett.* **6** 2748
[12] Lu Y H, Wu R Q, Shen L, Yang M, Sha Z D, Cai Y Q, He P M and Feng Y P 2009 *Appl. Phys. Lett.* **94** 122111
[13] Jippo H and Ohfuchi M 2013 *J. Appl. Phys.* **113** 183715
[14] Zhao X M, Wu Y J, Chen C, Ying Y and Kou S P 2016 *Chin. Phys. B* **25** 117303
[15] Yan W X 2013 *Chin. Phys. Lett.* **30** 047202
[16] Hu F, Duan L and Ding J W 2012 *Acta Phys. Sin.* **61** 077201 (in Chinese)
[17] Pan C N, He J and Fang M F 2016 *Chin. Phys. B* **25** 078102
[18] Kheyri A and Nourbakhsh Z 2016 *Chin. Phys. B* **25** 093102
[19] Wakabayashi K, Sasaki K I, Nakanishi T and Enoki T 2010 *Sci. Technol. Adv. Mater.* **11** 054504
[20] Son Y W, Cohen M L and Louie S G 2006 *Phys. Rev. Lett.* **97** 216803
[21] Kumar, T J D, Shukla A and Kumar R 2015 *Phys. Rev. B* **91** 115428
[22] Li Y, Jiang X W, Liu Z F and Liu Z R 2010 *Nano Res.* **3** 545
[23] Lü Y and Guo J 2010 *Nano Res.* **3** 189
[24] Zheng H X, Wang Z F, Luo T, Shi Q W and Chen J 2007 *Phys. Rev. B* **75** 165414
[25] Jiang L W, Zheng Y S, Yi C S, Li H D and Lü T Q 2009 *Phys. Rev. B* **80** 155454
[26] Onipko A 2008 *Phys. Rev. B* **78** 245412
[27] Shemella P, Zhang Y, Mailman M, Ajayan P M and Nayak S K 2007 *Appl. Phys. Lett.* **91** 042101
[28] Xie H, Kwok Y H, Zhang Y, Jiang F, Zheng X, Yan Y J and Chen G H 2013 *Phys. Status Solidi B* **250** 2481
[29] Castro E V, Peres N M R, Santos J M B L D, Neto A H C and Guinea F 2008 *Phys. Rev. Lett.* **100** 026802
[30] Huang W Q, Huang Z M, Cheng H Q, Miao X J, Shu Q, Liu S R, Qin C J 2012 *Appl. Phys. Lett.* **101** 171601
[31] Hadjisavvas G, Remediakis I N and Kelires P C 2006 *Phys. Rev. B* **74** 165419
[32] Michalak D J, Amy S R, Aureau D, Dai M, Estève A and Chabal Y J 2010 *Nature Materials* **9** 266271
[33] Lü X L, Liu Z, Yao H B, Jiang L W, Gao W Z and Zheng Y S 2012 *Phys. Rev. B* **86** 045410
[34] Liu Y, Song J T, Li Y X, Liu Y and Sun Q F 2013 *Phys. Rev. B.* **87** 195445
[35] Tang C L, Yan W H, Zheng Y S, Li G S and Li L P 2008 *Nanotechnology* **19** 435401
[36] Modarresi M, Roknabadi M R and Shahtahmasbi N 2011 *Physica E* **43** 1751
[37] Datta S 1995 *Electronic Transport in Mesoscopic Systems* (Cambridge: Cambridge University Press), p. 148